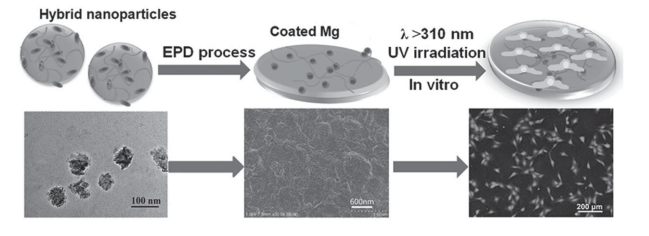


# A Biodegradable Coating Based on Self-Assembled Hybrid Nanoparticles to Control the Performance of Magnesium

Jiadi Sun, Ye Zhu, Long Meng, Tiantian Shi, Xiaoya Liu,\* Yufeng Zheng

A new biodegradable nanocomposite coating to control the biocompatibility and anticorrosion property of Mg is reported in this work. The key feature of this strategy is to equip the Mg surfaces with poly( $\gamma$ -glutamic acid)-q-7-amino-4-methylcoumarin/hydroxyapatite ( $\gamma$ -PGA-q-AMC/ HA) hybrid nanoparticles via electrophoretic deposition in ethanol. The microstructures of the resulting nanocomposite coating are characterized by Fourier transform infrared spectroscopy, X-ray diffraction, and scanning electron microscopy. The results of standard electrochemical measurements along with immersion tests indicate that the nanocomposite coating has preferable in vitro degradation and corrosion resistance behavior than bare Mg. In addition, cytocompatibility is conducted using NIH3T3 cells and the coated sample shows better cell viability and cell adhesion than pure Mg substrate over the whole incubation period. The

favorable anticorrosion behavior and cytocompatibility of the nanocomposite coating suggest that the newly developed  $\gamma$ -PGA-q-AMC/ HA biodegradable nanocomposite coating may have a potential to improve the biological performance of Mg-based biomedical implants.



#### 1. Introduction

Magnesium and its alloys have recently been considered as promising biodegradable bone fixation and repair implants because they are able to degrade on demand in vivo environment with the completion of their intended functions.[1-3] Moreover, Mg-based implants can lower

J. Sun, Dr. Y. Zhu, L. Meng, T. Shi, Prof. X. Liu Key Laboratory of Food Colloids and Biotechnology Ministry of Education School of Chemical and Material Engineering Jiangnan University Wuxi, Jiangsu 214122, P. R. China E-mail: lxy@jiangnan.edu.cn Prof. Y. Zheng Department of Materials Science and Engineering

State Key Laboratory for Turbulence and Complex System and College of Engineering

Peking University

Beijing 100871, P. R. China

long-term complications risk associated with permanent implants, such as foreign-body caused inflammatory response, delayed type hypersensitivity, and painful secondary removal surgery. [4-6] However, the most challenge of biodegradable Mg-based implants is their fast degradation rate in human ambient.[7,8] Although improving microstructure and composition of Mg-based implants by alloying and manufacturing methods are possible ways to control the corrosion behavior of Mg alloys, surface coating and modification techniques have become more promising because of the relative simpler approach with reasonable good results.[9,10]

In general, coatings on Mg surfaces include two categories, conversion coatings and degradable polymer coatings.[11] For Mg alloys, the most studied conversion coatings are calcium phosphate based,[12] although the biocompatibility of calcium phosphate coatings is generally higher than other conversion coatings (oxides, phosphates, or fluorides), the corrosion protection of these poor film-forming coatings is low because they

often display cracks or pores which result in unfavorable corrosion levels. Thus, sealing the pores of calcium phosphate based coatings is critical for their practical application. For coatings of degradable polymers, [13,14] they can not only act as a corrosion barrier but can be prepared with a wide range of properties and functions because of the infinite variability of their chemical composition and structures. However, although providing good protection and enhancing surface biocompatibility for the Mg stents, the polymer coatings did not maintain a reduction in corrosion rate over the long term due to their poor mechanical strength and inhomogeneous coating durability.

An ideal anticorrosion coating for Mg implants should not only provide corrosion resistance for the underlying alloys but also possess some additional functions, such as the enhancement of biocompatibility, bioactivity, and promoting tissue growth and healing.[15,16] Considering all these aspects, polymer-inorganic composite coatings appear especially interesting because of the diversity of their chemical and physical properties. The inorganic parts contribute to corrosion barrier ability of the resulting coatings. [17] And the bulk polymer constituents in the coating can provide good film-forming property, biological functions, and also corrosion barrier. [18,19] In the last few years, several polymer-inorganic coating were deposited onto Mg surfaces using different methods. Abdal-hay et al.<sup>[20]</sup> adopted a spraying approach to fabricate composite coating materials using hydroxyapatite (HA)-doped poly(lactic acid) on AZ91 Mg alloys. Wei et al.[21] combined plasma electrolytic oxidation and dipping techniques to create a polydopamine-assisted heparinized plasma electrolytic oxidation/poly(1-lactic acid) composite coating on biodegradable AZ31 alloy. Hahn et al.<sup>[22]</sup> utilized an aerosol deposition method to prepare hydroxyapatite-chitosan composite coatings on Mg alloy substrate. However, certain issues such as weak bonding to metallic substrates, maldistribution inorganic parts, and multistep coating fabrication process still exist which limit their practical applications.

Herein, one-step electrophoretic deposition (EPD) technique was used to fabricate protective nanocomposite coatings on Mg substrates. The EPD approach has attracted considerable attention, especially for biological applications, because it exploits the principle of charged particles or molecules in an applied electric field. [23-25] These advantages made EPD a versatile, simple method for incorporation of synthetic and natural biodegradable polymers and particles into biomedical coatings with strong interfacial bonding strength. [26,27] Since Mg alloys have high reaction rate with aqueous solutions during EPD process, which would prevent coating formation, to prepare desirable composite coatings on Mg surfaces, we performed an EPD process of self-assembled hybrid nanoparticle in ethanol solutions. In our previous work, [28,29] we applied this method to prepare good initial corrosion resistance and drug release functional nanostructured polymer coatings on Mg-Ca alloy surfaces. In this study, we further proposed a coating strategy of combining additional inorganic materials with self-assembled biopolymer particles to prepare better performance Mg-based composite coating surfaces. And HA was used as the inorganic part of the combination coating because of its excellent biocompatibility, bioactivity, and osteocoductivity. The overall fabrication procedure is illustrated in Figure 1. The inorganic HA, which is similar to native mineralized tissues, [30,31] were encapsulated into photocross-linking poly( $\gamma$ -glutamic acid)-g-7-amino-4methylcoumarin (γ-PGA-q-AMC) copolymers, forming γ-PGA-q-AMC/HA self-assembled hybrid nanoparticles. The nanostructured composite coating was fabricated by electrophoretic deposition of the particles. The successful deposition of  $\gamma$ -PGA-q-AMC/HA hybrid nanoparticles on the surfaces of Mg and phase compositions of the coated Mg samples were examined. The degradation process of bare and coated Mg samples was confirmed in simulated

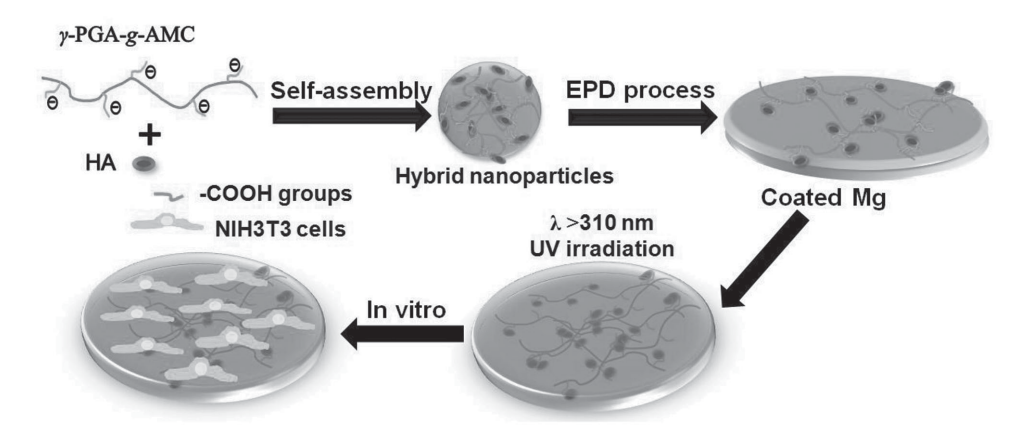


Figure 1. Schematic illustration of the Mg-based nanocomposite coating fabrication using self-assembled hybrid nanoparticles and EPD technique.





body fluid (SBF). And the activity and adhesion morphology of NIH3T3 normal cells on bare and coated Mg surfaces were also estimated.

## 2. Experimental Section

#### 2.1. Materials

Photocross-linking  $\gamma$ -PGA-q-AMC copolymers were prepared according to our reported procedure.[28] HA and fluorescein diacetate (FDA) were obtained from Aladdin Reagent Co., Ltd. (Shanghai, China). Konjac flour was acquired from Wanfeng Food Additive Co., Ltd. (Zhengzhou, China). Dimethyl sulfoxide (DMSO), absolute ethanol, and triethylamine were acquired from Sinopharm Chemical Reagent Co., Ltd. (Shanghai, China). Mouse NIH3T3 cells were purchased from Cell Resource Center of Chinese Academy (Shanghai, China). Dulbecco's modified Eagle's medium (DMEM: Gibco), fetal bovine serum (Hyclone), 3-(4,5-dimethylthiazol-2-yl)-2,5-diphenyltetrazolium (MTT: biotopped), and antibiotics (Gibco) were purchased from Wuxi Trivd Biotechnology Inc. (Wuxi, China). These chemical agents and solvents were used without further purification. The Mg substrate (composition: 100% Mg, diameter 9.5 mm, 1.5 mm thick) were donated by Zheng and co-workers.[32]

## 2.2. Preparation of $\gamma$ -PGA-g-AMC/HA Hybrid Nanoparticles

HA powders (3 mg) were added into 5 mL DMSO in 10 mL glass beaker and ultrasonically treated for 3 h to ensure its homogeneous distribution. The  $\gamma PGA-g$ -AMC (25 mg) was dissolved in 5 mL DMSO to form copolymer solution. After these, the two kinds of solutions mentioned above were mixed and stirred for 1 h at 25 °C and we got  $\gamma PGA-g$ -AMC/HA composite solution. To prepare  $\gamma PGA-g$ -AMC/HA hybrid nanoparticles, double volume of absolute ethanol was added dropwise into the composite solution to promote self-assembled process of the system. The resulting particle solution was dialyzed against ethanol to remove DMSO and a stable  $\gamma PGA-g$ -AMC/HA hybrid nanoparticle solution was obtained.

The hybrid nanoparticles were characterized for particle size using dynamic light scattering (DLS) with a combination BIC 90Plus and ZetaPALS instrument (Brookhaven Instruments Corp., USA). Prior to the measurement, the sample was filtered through 0.8  $\mu m$  Millipore filters and each measurement was conducted in triplicate. Morphology of the particles was obtained on a JEOL JEM-2100 transmission electron microscope (TEM) at a 200 kV accelerating voltage. The TEM sample was prepared by dropping diluted particle solution onto copper grids and then drying it at room temperature.

## 2.3. Fabrication of Nanostructured Composite Coating Using EPD

The Mg plate was polished by SiC paper to 1200 grit, ultrasonically cleaned in 20 mL alcohol, and 20 mL acetone, respectively, and then dried at room temperature. Prior to the deposition, the

pH value of the  $\gamma$ -PGA-g-AMC/HA hybrid nanoparticle solution was adjusted to 7–8 by triethylamine. The EPD process was conducted in a 50 mL EPD cell at a 150 V constant voltage and 30 min deposition time, with an Mg substrate (anode) and a Pt electrode (cathode). After this, the coated sample was removed carefully from the EPD cell and dried horizontally in air at room temperature overnight.

The presence of the nanocomposite coating was confirmed by attenuated total reflectance Fourier transform infrared spectroscopy (ATR-FTIR) ranging from 400 to 4000 cm $^{-1}$  (Nicolet 6700, Thermo Electron Corp., Madison, WI, USA). X-ray diffraction (XRD) instrument (D8, Bruker, Karlsruhe, Germany) with a Cu K $\alpha$  radiation was carried out to probe the structure of coated and bare Mg samples, the measurement was operated from 3° to 90° with steps of 0.02° at a scan rate of 4° min $^{-1}$ . The microstructural observations of the coating surface were studied by scanning electron microscopy (SEM) at 2.0 kV (model S-4800, Hitachi, Tokyo, Japan).

## 2.4. Electrochemical Corrosion Analysis

Before conducting the measurement, the coated Mg sample was irradiated for 30 min with a UV curing system (1000 W, 365 nm), in order to fabricate a photocross-linked smooth surface of the coated sample. The corrosion test was conducted in a standard SBF (NaCl: 8.036 g L-1, NaHCO3:  $0.352 \text{ g L}^{-1}$ , KCl:  $0.225 \text{ g L}^{-1}$ ,  $K_2HPO_4 \cdot 3H_2O$ :  $0.230 \text{ g L}^{-1}$ , MgCl<sub>2</sub>·6H<sub>2</sub>O: 0.311 g  $L^{-1}$ , 1.0 M HCl: 40 mL  $L^{-1}$ , CaCl<sub>2</sub>: 0.293 g  $L^{-1}$ , Na<sub>2</sub>SO<sub>4</sub>: 0.072 g L<sup>-1</sup>, tris(hydroxylmethyl) aminomethane: 6.063 g L<sup>-1</sup>) at a pH of 7.4, and the temperature was controlled at 37  $\pm$  0.5 °C. [33] A three-electrode cell system was used to carry out the measurements (CS350, Wuhan Corrtest Instrument Co., Ltd, China). The coated and photocross-linked samples, a platinum plate, and a saturated calomel electrode were used as working, counter, and reference electrodes, respectively. The recording range was from -0.6 to 0.6 V of the open-circuit potential at a scanning rate of 1 mV s<sup>-1</sup>.

#### 2.5. Immersion Test

The in vitro degradation characteristics of bare Mg and coated Mg substrates were carried out at different time points. Before the experiment, the coated Mg sample was irradiated with UV light to improve the coating barrier property. The treated and untreated Mg samples were individually immersed into sealed bottle containing 30 mL SBF and then incubated at 37  $\pm$  0.5  $^{\circ}\text{C}$ for a total of 2 months.[19] The experiments for the treated and untreated Mg samples were performed independently in triplicate, respectively. The release amount of Mg ions from each sample was measured at predetermined time intervals using atomic absorption spectrophotometer (TAS-990NFG, China). The correlation between Mg ion dissolution and immersion time was subsequently established. In addition, the pH values of different samples were also measured with a pH measuring instrument. The surface morphology of different immersed samples were investigated using ultradepth of field 3D microscope (VHX-1000C, Keyence, Hong Kong) and XRD was carried out to probe the phase structure of each immersed sample.





To simulate the corrosion process of bare and coated Mg in human tissue, different samples were embedded into konjac flour gels. At different time (1, 3, 5, and 10 d), photographs of uncoated and coated samples were obtained. The process was described as follows: 15 g konjac flour and 200 mL SBF solutions were added to a 500 mL beaker. The konjac flour SBF solution was boiled for 5 min with a heating device. The bare and coated Mg were placed into six-well plates, and then the above boiled solution was poured into each well. After the samples were cooled down at room temperature, the gels containing bare and coated Mg substrates were obtained, respectively.

#### 2.6. Cell Culture

### 2.6.1. Cell Viability Test of the Immersion Extracts

The MTT assay was used to determine the cell viability of the coated and uncoated Mg. The measurement was conducted using an indirect method, where the immersion extracts collected from the immersion test were used for cell culture.[34] Before cell incubation, the immersion extracts were sterilized using 0.2 µm Millipore filters. NIH3T3 cells were seeded into 96-well plates with a density of  $6 \times 10^3$  cells per well in 100  $\mu L$ DMEM medium supplemented with 10% fetal bovine serum and 1% antibiotics. The cells were cultured for 1 d in a humidified atmosphere of 5% CO<sub>2</sub> at 37 °C. On the second day, the culture medium in each well were replaced with 50 µL immersion SBF extracts and 50 µL DMEM medium containing 10% fetal bovine serum and 1% antibiotics. Culture medium without the extract served as the negative control and 5% DMSO containing culture medium as the positive control. After incubating for 2 d, cell morphologies of different samples were obtained using an inverted optical microscope (CKX41, Olympus, Olympus America Inc.). Then, 10  $\mu L$  of 5 mg mL<sup>-1</sup> MTT solution was added into each well. The 96-well tissue culture plates were incubated for a further 4 h. After incubation, formazan was formed and dissolved in 100 µL of DMSO per well. The absorbance was measured with a multimode detector (Tecan Infinite M200 PRO, Shanghai DoBio Biotech. Co., Ltd) at a wavelength of 570 nm referenced to 630 nm. The cell viability was calculated using following equation: cell viability (%) =  $(OD_{sample}/OD_{negative\ control}) \times$ 100%

## 2.6.2. Cell Adhesion with Direct Incubation on Various Surfaces

NIH3T3 cells were maintained in DMEM medium supplemented with 10% fetal bovine serum and 1% antibiotics at 37 °C. Before cell seeding, bare Mg substrate was sterilized under UV light for 1.5 h on each side and the coated sample was sterilized by UV cross-linking process. NIH3T3 cells were seeded onto the surfaces of different samples in a 24-well plate at a density of 6  $\times$  10 $^4$  cells per well with 500  $\mu L$  of DMEM medium containing 10% fetal bovine serum and 1% antibiotics in a humidified atmosphere of 5% CO $_2$  at 37 °C. The cells were cultured for 5 and 24 h, respectively.

At different culturing time, 1  $\mu L$  of 5 mg mL<sup>-1</sup> FDA acetone solution was added in each well to stain the cells for 15 min. The stained samples were then rinsed twice with sterile phosphate

buffered saline (PBS) and the cell images were captured with a fluorescence microscope under green filter (Nikon 80i, Japan). In addition, after being cultured for 24 h, the cells were fixed using a 2.5 vol% glutaraldehyde solution for 2 h at 37 °C. Subsequently, the samples were washed with PBS for twice and then immersed in 10%, 20%, 30%, 40%, 50%, 60%, 70%, 80%, 90%, and 100% (v/v) ethanol/water solutions for 10 min, respectively. [35] The adhesion morphologies of NIH3T3 on each sample were observed by an ultradepth of field 3D microscope (VHX-1000C, Keyence, Hong Kong) after drying.

The cell viability of NIH3T3 cells on the various sample surfaces was also evaluated using MTT assay. After 24 h cultivation, samples were rinsed with PBS for two times. A 500  $\mu L$  fresh DMEM medium containing 5 vol% MTT (5 mg mL $^{-1}$  in PBS) replaced the previous culture medium. After being incubated for another 4 h, the culture media were removed and 500  $\mu L$  DMSO was added to each sample to dissolve the formazan. The absorbance of different sample solutions was measured at 570 nm referenced to 630 nm using a multimode detector (Tecan Infinite M200 PRO, Shanghai DoBio Biotech Co., Ltd).

#### 2.6.3. Statistical Analysis

All of the biological measurements were conducted independently in quadruplicate (n=4), and three replicates were performed for each experimental point. Statistically significant differences (p) between the various groups were measured using one-way analysis of variance and all the data were expressed as the mean  $\pm$  standard deviation.

## 3. Results and Discussion

## 3.1. Preparation of $\gamma$ -PGA-g-AMC/HA Hybrid Nanoparticles

To study the self-assembly behavior of  $\gamma$ -PGA-q-AMC and HA,  $\gamma$ -PGA-g-AMC/HA hybrid nanoparticles were prepared by slowly adding ethanol dropwise into DMSO mixture solutions of  $\gamma$ -PGA-q-AMC and HA under vigorous stirring. The hydrodynamic diameter  $(D_h)$  and distribution index of the hybrid nanoparticles were measured. The size and its distribution of the particles are shown in Figure 2A, the average  $D_h$  value of the hybrid nanoparticle was determined to be around 180 nm with low polydispersity, and the particle solution shown classic blue opalescence of colloidal particle solution. The morphology and size of the particles in dry state were observed by TEM. As shown in Figure 2B, the  $\gamma$ -PGA-g-AMC/HA hybrid nanoparticles were aggregates with an average diameter of 90 nm, which was smaller than the size measured by DLS. This reduced diameter can be attributed to the difference between the dried and hydrated states of the nanoparticles. In addition, the HA particles were encapsulated into the nanoparticles as clearly seem from TEM image. The formation process of these nanoparticles may be described as follows





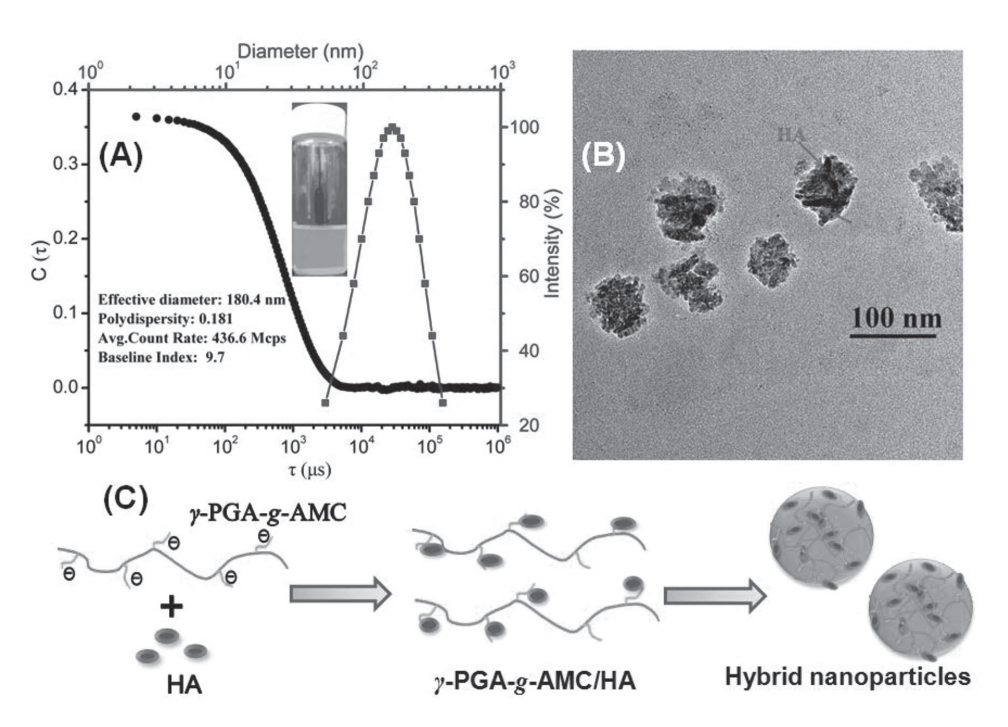


Figure 2. Hydrodynamic diameter A), TEM image B), and illustration of the proposed mechanism C) for the self-assembly of  $\gamma$ -PGA-g-AMC/HA hybrid nanoparticles.

(Figure 2C):  $\gamma$ -PGA-g-AMC is negative charged because of containing plenty of –COOH groups, and HA was positive charged. When they were mixed together, HA can absorb on the  $\gamma$ -PGA-g-AMC main chains due to the presence of electrostatic force. With the addition of ethanol,  $\gamma$ -PGA-g-AMC/HA main chains started to collapse into insoluble complexes because of hydrogen bonding between polymer chains, thus forming  $\gamma$ -PGA-g-AMC/HA hybrid nanoparticles.

#### 3.2. Fabrication of Nanocomposite Coating Using EPD

Nanocomposite coating onto Mg was obtained by EPD in the  $\gamma$ -PGA-g-AMC/HA hybrid nanoparticle ethanol solution. The proposed coating formation mechanism was based on the classical Derjaguin–Landau–Verwey–Overbeek theory of colloidal particle stability. Simply put, as shown in Figure S1 (Supporting Information), the hybrid nanoparticles were stable dispersion in ethanol medium because of the energy barrier between particles. When an electric field was applied, the negatively charged  $\gamma$ -PGA-g-AMC/HA hybrid nanoparticles would migrate, and the migration can induce a particle concentration gradient around the Mg surfaces. While the energy barrier between these nanoparticles around the Mg anode was overcome in the applied electric field, coagulation became possible and the nanocomposite coating would be formed. [37–39]

ATR-FTIR was used to verify the presence of the nanocomposite coating on the metal surface. The original Mg sample demonstrated a chemical inertness surface as displayed in Figure 3A. The characteristic peaks of symmetric C=O stretching for -COOH and -CO-NH- groups, and C=C stretching of AMC groups in raw  $\gamma$ -PGA-g-AMC spectrum were clearly visible at 1726, 1655, and 1534 cm<sup>-1</sup>, respectively. Meanwhile, from the ATR-FTIR spectrum of pristine HA, the characteristic peak of PO<sub>4</sub><sup>3-</sup> vibrations appeared at 562 and 1030 cm<sup>-1.[40]</sup> More importantly, these mentioned peaks have been shown in the spectrum of the nanocomposite coating. The results provided good evidence that the  $\gamma$ -PGA-g-AMC/HA hybrid nanoparticles were embedded on Mg surfaces. XRD patterns of the selected products including the original HA, bare Mg, and nanocomposite coating modified Mg sample were shown in Figure 3B. Compared to bare Mg, the coated Mg sample also displayed major characteristic diffraction peaks of Mg phase, and as expected, the peak intensity decreased due to the formation of nanocomposite coating on Mg surfaces. These results indicated that the  $\gamma$ -PGA-g-AMC/ HA nanocomposite coating was prepared successfully and the original Mg could be coated by  $\gamma$ -PGA-q-AMC/HA hybrid nanoparticles through EPD process in ethanol.

The surface observations for different samples were investigated by SEM. The results are shown in Figure 4. The bare Mg surfaces were roughness, which caused by the polishing process of pretreatment. The morphology of nanocomposite coating was uniform and the particle stacking morphology could be clearly seen before UV irradiation (Figure 4B). This indicates that homogeneous





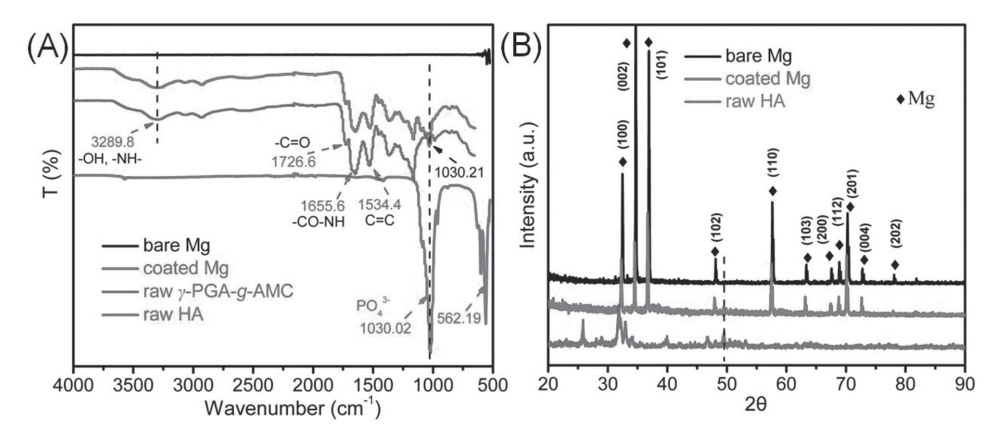


Figure 3. ATR-FTIR spectra A) and XRD patterns B) of bare Mg, coated Mg sample, raw γ-PGA-g-AMC, and raw HA.

nanocomposite coating was fabricated by EPD of self-assembled hybrid nanoparticles. In addition, there are some pores on the surfaces of coated Mg sample, it may be caused by the evaporation of ethanol and the shrinkage of nanocomposite coating during the coating drying process in air. After UV irradiation for 30 min, the coating surface became flat and smooth because of the photocross-linking properties of the coumarin (AMC) groups in the coating (Figure 4C). [41–43] And coating thickness was determined by light microscope image at cross-section of the coated Mg, the outcome displayed that the coating thickness was around 100  $\mu m$  (marked by the arrows in Figure 4D). The above results clearly showed that nanocomposite coating formed on the Mg and further UV irradiation process could smooth the surface morphology

## 3.3. Corrosion Analysis

of the resultant coating materials.

The corrosion resistance of the coatings on Mg-based materials is critical for their applications. As partial swelling of nanocomposite coating may occur in aqueous solution because of water absorption, further UV cross-linking modification may have a beneficial effect on corrosion resistance of the nanocomposite coating, because the barrier property of the coating were improved.[44-46] Figure 5 shows the potentiodynamic polarization curves of bare Mg, coated Mg, and surface UV cross-linked Mg sample in SBF, the inset table summarizes the corrosion potential  $(E_{corr})$  and corrosion rate  $(R_{corr})$ calculated from extrapolation of the Tafel plots. All of the coated samples presented better corrosion resistance, while the bare Mg exhibited high chemical reactivity in SBF with low corrosion potential (-1.80 V) and high corrosion rate ( $24.69 \text{ mm y}^{-1}$ ). After being coated with nanocomposite coating, the sample showed much more positive corrosion potential (-1.55 V) and lower corrosion rate ( $16.96 \text{ mm y}^{-1}$ ). As expected, the photocross-linked nanocomposite coating showed better protection for the Mg substrate with relatively positive corrosion potentials (-1.46 V) and lower corrosion rate ( $10.98 \text{ mm y}^{-1}$ ). Therefore, both the  $E_{\text{corr}}$  and  $R_{\text{corr}}$  indicated that the initial corrosion resistance of Mg was affected by the composite coating and further UV irradiation process. These observed differences in electrochemical data among the tested samples are a consequence of difference in the coating chemical structure. Before UV irradiation, molecular

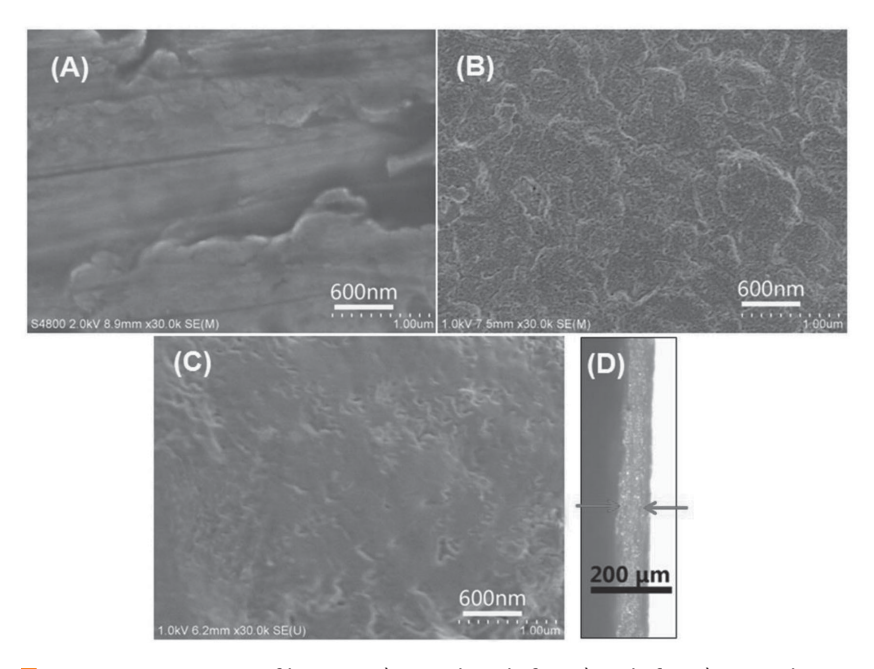


Figure 4. SEM images of bare Mg A), coated Mg before B), and after C) UV irradiation. The cross-section light microscope picture D) of coated sample after UV irradiation. The UV irradiated time is 30 min (1000 W, 365 nm).





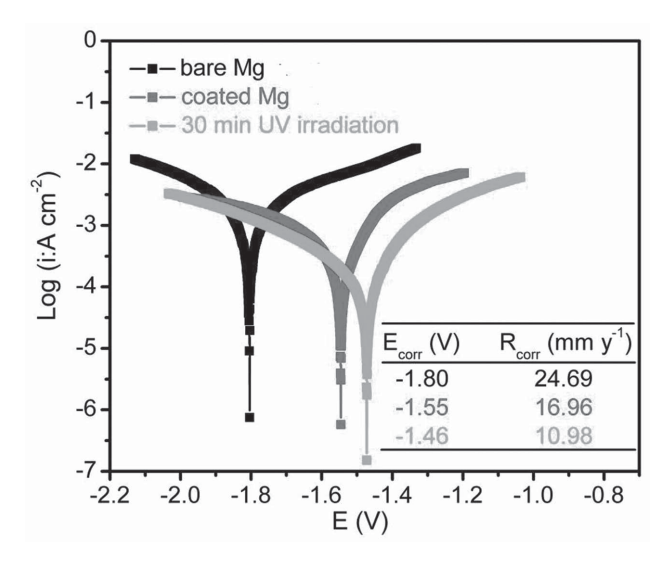


Figure 5. The polarization curves for different samples in 37  $\pm$  0.5 °C SBF, pH = 7.4. The inside is the corrosion potential ( $E_{corr}$ ) and corrosion rate ( $R_{corr}$ ) values for different samples.

chains in the coating are mainly hydrogen and electrostatic bonding. With UV irradiation, additional chemical bonding networks were formed in the coating, resulting in a more stable coating layer and a stronger anticorrosion ability. [45,46]

#### 3.4. Immersion Test

The degradation behaviors of bare Mg and coated Mg after UV irradiation were observed by immersion different samples in SBF. While the pure Mg sample is degraded only due to the corrosion reaction of Mg, the degradation of coated sample was related to both the Mg corrosion and dissolution of coating layers. [47,48] Figure 6 shows the

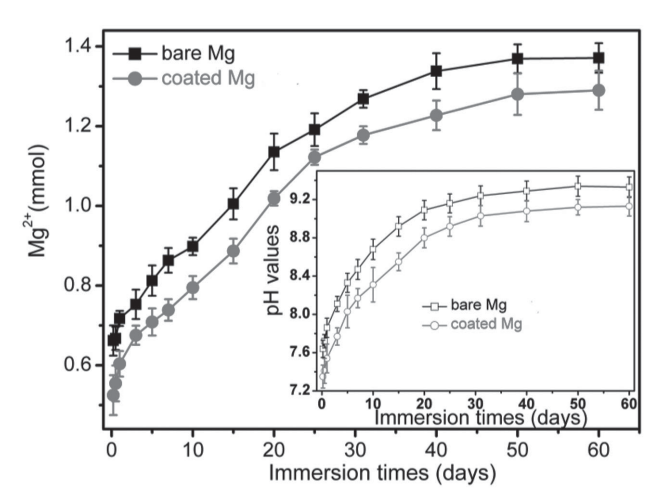


Figure 6. Released Mg ion concentrations from uncoated and coated Mg samples in 37 °C SBF at different immersion days, the inside is the pH values.

concentration of Mg ions released and pH values of bare and coated Mg samples, respectively. During the whole immersion time, the higher Mg ion concentrations were released form bare Mg sample, compared to that of the coated sample. And the pH values of the SBF solution was measured up to 60th day as pH data could also reflect the corrosion behavior of Mg samples, and the result was shown in the inset picture. The in vitro corrosion of bare Mg followed the general reaction, thus causing an alkaline atmosphere which led to higher pH values over the whole testing period, compared to that of the coated Mg sample. This means that nanocomposite coating provided good corrosion protection to the Mg matrix during the immersion period. It attributed to the fact that the coating on Mg surface could isolate the underlying substrate from SBF erosion at the initial immersion time, and inhibit the shedding and dissolution of corrosion products in the latter part of immersion time. [49] Meanwhile, compared to our previous results, [28,29] this nanocomposite coating material can act as better anticorrosion layers of Mg-based implants.

The life of the coating according to the morphology was identified by a light microscope at different immersion days and the XRD patters were also obtained. As shown in Figure 7, light microscopy images of the uncoated Mg sample (A1 and A2) showed the characteristic corrosion surface morphology of Mg after immersing in SBF for 30 and 60 d, respectively. However, the coated substrate displayed various levels of corrosion progression, the bulk of Mg sample were still coated in nanocomposite coating with some underlying corrosion products after the immersion time of 30 d (B1). The portion of nanocomposite coating remained and the bulk of corrosion products on Mg surfaces were exposed after 60 d (B2). These results confirmed that the nanocomposite coating could inhibit the shedding and dissolution of corrosion products during immersion process. The XRD patterns (C1 and C2) indicated that the main corrosion products were inorganic oxide, and compared to bare Mg, the coated Mg could maintain nearly complete cylindrical shape as reflected from the inset digital photographs. In addition, the compressive strengths of bare and coated samples were  $\approx$ 109  $\pm$  5.7 and 164  $\pm$  4.8 MPa after immersing in SBF for 60 d, respectively. The results displayed that the nanocomposite coating not only improved the corrosion resistance of Mg but also protected mechanical strength of Mg substrate, while the mechanical integrity of Mg-based stents is critical for their performance as bone implants.

To visualize the degradation process of bare and coated Mg, the samples were encapsulated into gels fabricated by SBF and konjac flour, the results were shown in Figure 8. As the images shown, there are many bubbles around bare Mg sample during 1 d encapsulation in gels. It indicated that the pure Mg was corroded by





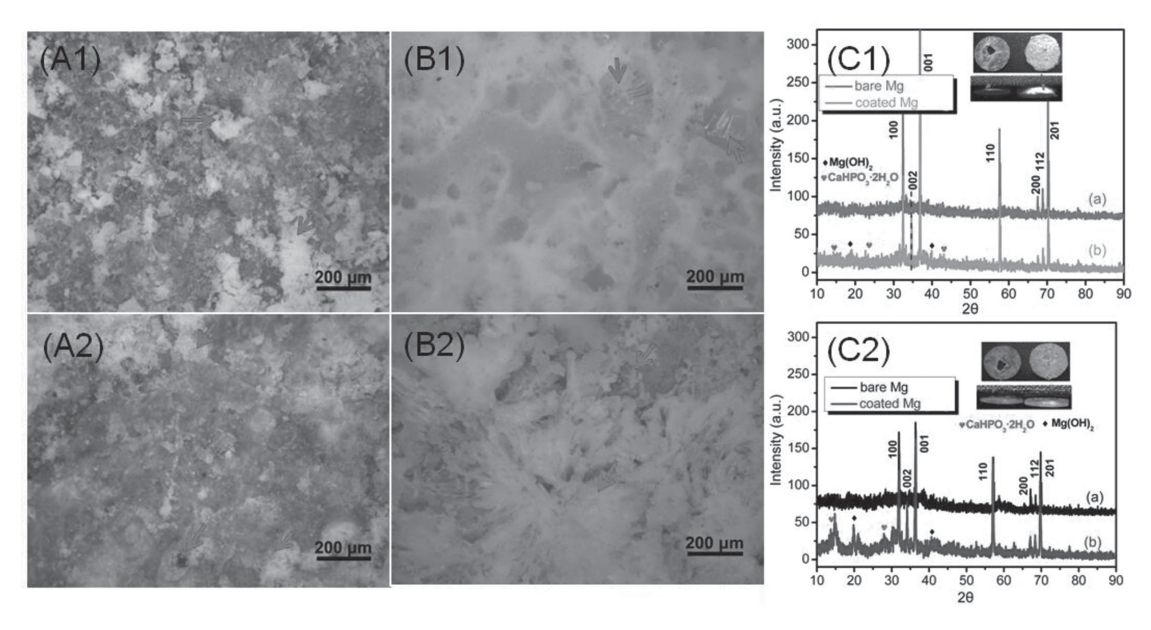


Figure 7. Light microscope images A1,A2,B1,B2) and XRD patterns C1,C2) of bare Mg A1,A2) and coated Mg sample B1,B2) after immersion of 30 d A1,B1,C1) and 60 d A2,B2,C2) in SBF at 37 °C with pH = 7.4.

SBF gels and the corrosion product  $\rm H_2$  gas was released. The  $\rm H_2$  bubbles around bare Mg continued to increase in 3 d. However, the released  $\rm H_2$  bubbles of bare Mg sample slightly increased from 3 to 10 d, it was due to the fact that the produced gas separated the Mg substrate from the SBF gels. For coated Mg sample, the released bubbles were inconspicuous until 10 d. The digital photographs of different samples encapsulated in SBF gels after 10 d were shown in Figure S2 (Supporting Information), the result showed that some white corrosion products have formed on bare Mg surfaces, but for the coated sample,

the coating still completely existed on the Mg surfaces. From these results, we can predict that the nanocomposite coating would alleviate the damage of subcutaneous bubbles while using it in live body, especially in the initial period.

The protection mechanism of the coated Mg sample can be summarized as partial degradation of the coating (a), localized corrosion of the substrate (b), formation of corrosion products (c), and shedding of the coating (d), which are schematically illustrated in Figure S3 (Supporting Information).<sup>[50,51]</sup> At the initial immersion period, the

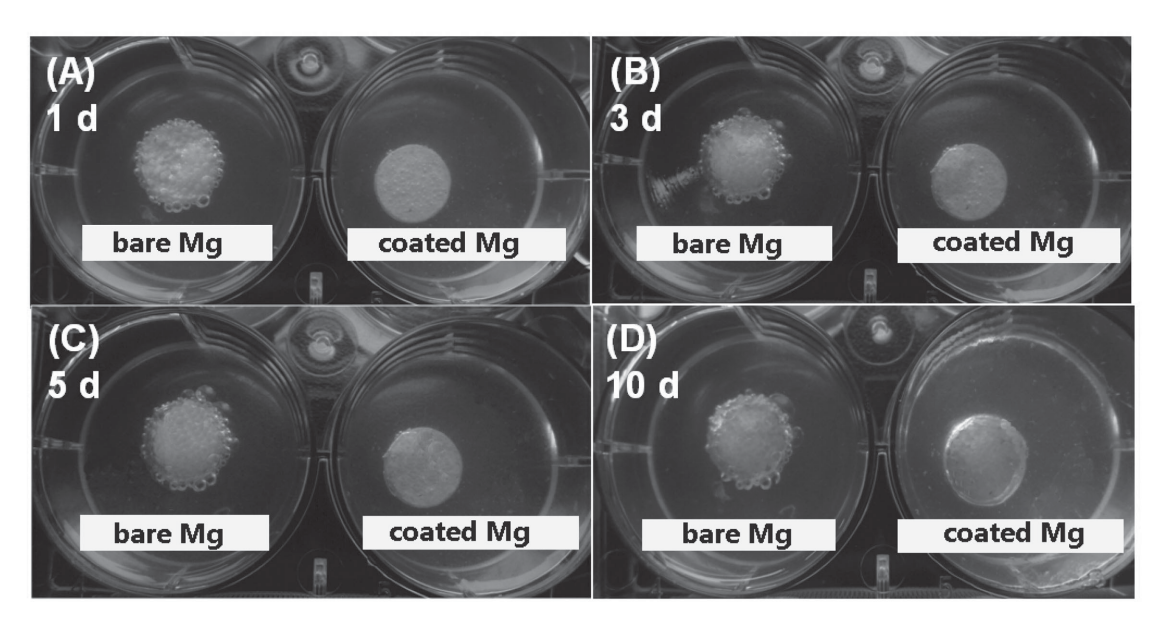


Figure 8. Digital photographs of bare Mg and coated Mg sample after embedding the samples in konjac flour gels for different days.





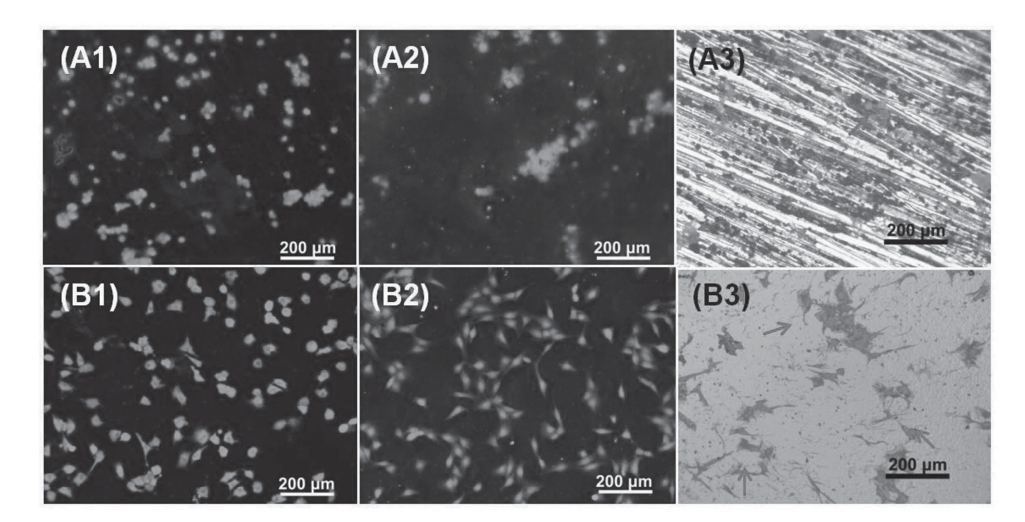


Figure 9. Fluorescent images A1,A2,B1,B2) and light microscope images A3,B3) of NIH3T3 cells after culturing for 5 h A1,B1) and 24 h A2,A3,B2,B3) on bare Mg A1,A2,A3) and coated Mg samples B1,B2,B3).

nanocomposite coating could physically isolate the underlying Mg substrate from the SBF corrosive solution. With an extension of immersion time, the weak points of the coating would produce microcracks under the erosion of SBF solution. Then SBF permeated into the coating through these cracks and corroded Mg substrate with the release of Mg<sup>2+</sup>, OH<sup>-</sup>, and H<sub>2</sub>. This release behavior of Mg substrate resulted in more cracks and pores through the outer layer coating, which would accelerate the degradation rate of the coated sample. When the released OHachieved high concentrations, corrosion products would form due to the sedimentation reaction of calcium, Mg, and phosphate ions. At this stage, the coating could slow the diffusion of the underlying corrosion products and decrease the corrosion rate of the coated Mg. During the latter part of immersion time, the surface coating would be stripped because of stress acts, which induced by corrosion process.

### 3.5. Cell Culture

## 3.5.1. Cell Viability Test of the Immersion Extracts

Cell viability is a critical aspect in the cytocompatibility evaluation of new biomaterials. Figure S4 (Supporting Information) shows the cell morphology and viability of positive group, negative group, bare Mg, and coated Mg sample. After incubation with the extracts for 2 d, the morphology of cells cultured with immersion extracts of bare (C) and coated (D) Mg exhibit an elongated and flattened spindle shape, which similar to that of the negative group (B). The cell viability for different samples was further evaluated by MTT assay, as Figure S4E (Supporting Information) shown, compared to negative group, the extracts of bare and coated Mg showed higher cell viability, because

the released  $Mg^{2+}$  ions from corrosion process of Mg substrates could promote the cellular metabolism and growth. However, the cell viability for extracts of coated Mg sample was significantly (p < 0.05) improved relative to that of bare Mg, which might be ascribed to the corrosion resistance increased by nanocomposite coating modification. As corrosion resistance increased, few ions ( $OH^-$  and  $Mg^{2+}$ ) would be released into the culture medium, thus resulting in a more suitable environment for cell growth. These results show that the concentrations of corrosion product were related to cell viability and confirm that the nanocomposite coating presented better cytocompatibility.

### 3.5.2. Cell Adhesion on Various Surfaces

Cell adhesion on the scaffolds is essential to the development and remodeling of biomedical engineering tissues. Adhesive interactions play a critical role in cell survival, proliferation, matrix mineralization, and tissue formation. To determine the cytocompatibility and cell adhesion capability of the nanocomposite coating, NIH3T3 cells were seeded and cultured for 24 h on bare and coated Mg samples, then cells were imaged using fluorescence and light microscopy. The results are shown in Figure 9, a few cells were found to attach on bare (A1) and coated (B1) Mg samples after culturing for 5 h. However, when the incubation time increased to 24 h, the NIH3T3 cells on coated Mg sample (B2 and B3) exhibited better adhesion and spread compared with those on bare Mg surfaces (A2 and A3). This phenomenon was attributed to the reason that bare Mg was chemically active and easily reacted with DMEM medium, which had a negative influence on cell attachment and spread. [55] As demonstrated in Figure S5 (Supporting Information), the proliferation of NIH3T3 cells on various surfaces revealed the same trend as that observed





for cell morphology. Thus, compared with bare Mg, the coating modified surfaces were more suitable for cell proliferation. Generally, cell adhesion, spreading, proliferation, and migration on substrates were the first sequential reactions while cells came into contact with material surfaces. Therefore, the observed extensive spread and attachment of NIH3T3 cells on the nanocomposite coating illustrated that the coating modified sample had a better biological property than bare Mg sample.

### 4. Conclusion

A biodegradable nanocomposite coating was deposited onto Mg substrate by electrophoretic deposition of selfassembled  $\gamma$ -PGA-q-AMC/HA hybrid nanoparticles. The particles could form a smooth, dense, and continuous coating layer on Mg substrate, which masked the groove feature on the Mg substrate surfaces. Standard electrochemical measurements (corrosion potential and corrosion rate) demonstrated that the nanocomposite coating, especially the photocross-linked coating layers, had an advantage in corrosion resistance behavior. Furthermore, the level of retention of surface morphology integrity, pH value change as well as the amount of Mg ions released in a controlled manner in vitro environment also indicated that the nanocomposite coating improved the corrosion resistance performance of Mg sample. In addition, NIH3T3 cells showed better cell viability and cell function adhered onto the coated Mg substrate than bare Mg. Therefore, the current in vitro data suggested that the developed biodegradable γ-PGA-q-AMC/HA nanocomposite coating may have the potential as surface coating materials for Mg-based biomedical implants to improve their anticorrosion property and biological performance.

## **Supporting Information**

Supporting Information is available from the Wiley Online Library or from the author.

Acknowledgements: This work was supported by the National Nature Science Foundation of China (NSFC) (under Grant Nos. 20974041 and 21174056), the Fundamental Research Funds for the Central Universities (JUSRP 51305A), MOE and SAFEA for the 111 Project (B13025), and funds from the Jiangsu postgraduate scientific research and innovation plan project (under Grant No. KYLX\_1128).

Received: June 16, 2015; Published online: September 3, 2015; DOI: 10.1002/macp.201500214

Keywords: biodegradable; EPD; Mg; nanocomposite coating; self-assembly

- [1] F. Witte, J. Fischer, J. Nellesen, H. A. Crostack, V. K. Pisch, F. Beckmann, H. Windhagen, *Biomaterials* **2006**, *27*, 1013.
- [2] Y. F. Zheng, X. N. Gu, N. Li, W. R. Zhou, Mater. China 2011, 30, 30.
- [3] M. P. Staiger, A. M. Pietak, J. Huadmai, G. Dias, *Biomaterials* 2006, 27, 1728.
- [4] G. S. Wu, J. M. Ibrahim, P. K. Chu, Surf. Coat. Technol. 2013, 233, 2
- [5] W. D. Mueller, M. L. Nascimento, M. F. L. Mele, Acta Biomater. 2010, 6, 1749.
- [6] F. Witte, V. Kaese, H. Haferkamp, E. Switzer, A. Meyer-Lindenberg, C. J. Wirth, H. Windhagen, *Biomaterials* 2005, 26, 3557.
- [7] Y. F. Zheng, X. N. Gu, F. Witte, Mater. Sci. Eng. R 2014, 77, 1.
- [8] F. Witte, N. Hort, C. Vogt, S. Cohen, K. U. Kainer, R. Willumeit, F. Feyerabend, Curr. Opin. Solid State Mater. Sci. 2008, 12.63.
- [9] R. G. Hu, S. Zhang, J. F. Bu, C. J. Lin, G. L Song, Prog. Org. Coat. 2012, 73, 129.
- [10] S. Shadanbaz, G. J. Dias, Acta Biomater. 2012, 8, 20.
- [11] Y. J. Chen, Z. G. Xu, C. Smith, J. Sankar, Acta Biomater. 2014, 10, 4561.
- [12] H. Hornberger, S. Virtanen, A. R. Boccaccini, Acta Biomater. 2012. 8, 2442.
- [13] H. M. Wong, K. W. K. Yeung, K. O. Lam, V. Tam, P. K. Chu, K. D. K. Luk, K. M. C. Cheung, *Biomaterials* 2010, 31, 2084.
- [14] C. Pfaffenroth, A. Winkel, W. Dempwolf, L. J. Gamble, D. G. Castner, M. Stiesch, H. Menzel, *Macromol. Biosci.* 2011, 11, 1515.
- [15] P. Lu, H. Fan, Y. Liu, L. Cao, X. Wu, X. H. Xu, Colloids Surf. B 2011, 83, 23.
- [16] P. Lu, Y. Liu, M. Q. Guo, H. D. Fang, X. H. Xu, Mater. Sci. Eng. C 2011, 31, 1285.
- [17] Y. Hu, X. Y. Gu, Y. Yang, J. Huang, M. Hu, W. K. Chen, Z. Tong, C. Y. Wang, ACS Appl. Mater. Interfaces 2014, 6, 17166.
- [18] F. Siedenbiedel, A. Fuchs, T. Moll, M. Weide, R. Breves, J. C. Tiller, Macromol. Biosci. 2013, 13, 1447.
- [19] S. Kunjukunju, A. Roy, M. Ramanathan, B. Lee, J. E. Candiello, P. N. Kumta, Acta Biomater. 2013, 9, 8690.
- [20] A. Abdal-hay, N. A. M. Barakat, J. K. Lim, Ceram. Int. 2013, 39, 183.
- [21] Z. L. Wei, P. Tian, X. Y. Liu, B. X. Zhou, Colloids Surf. B 2014, 121, 451.
- [22] B. D. Hahn, D. S. Park, J. J. Choi, J. Ryu, W. H. Yoon, J. H. Choi, H. E. Kim, S. G. Kim, Surf. Coat. Technol. 2011, 205, 3112.
- [23] R. Ma, R. F. Epand, I. Zhitomirsky, Coll. Surf. B 2010, 77, 279.
- [24] I. Krylova, Prog. Org. Coat. 2001, 42, 119.
- [25] R. Fernandes, L. Q. Wu, L. H. Chen, H. Yi, G. W. Rubloff, R. Ghodssi, W. E. Bentley, G. F. Payne, *Langmuir* 2003, 19, 4058.
- [26] S. Seuss, A. R. Boccaccini, Biomacromolecules 2013, 14, 3355.
- [27] Z. L. Wang, X. Q. Zhang, J. M. Gu, H. T. Yang, J. Nie, G. P. Ma, Carbohydr. Polym. 2014, 103, 38.
- [28] J. D. Sun, X. Y. Liu, L. Meng, W. Wei, Y. F. Zheng, Langmuir 2014, 30, 11002.
- [29] J. D. Sun, Y. Zhu, L. Meng, W. Wei, Y. Li, X. Y. Liu, Y. F. Zheng, J. Mater. Chem. B 2015, 3, 1667.
- [30] M. Li, Q. Liu, Z. J. Jia, X. C. Xu, Y. Cheng, Y. F. Zheng, T. F. Xi, S. C. Wei, *Carbon* 2014, 67, 185.
- [31] M. Li, Y. B. Wang, Q. Liu, Q. H. Li, Y. Cheng, Y. F. Zheng, F. F. Xia, S. C. Wei, J. Mater. Chem. B 2013, 1, 475.
- [32] Z. J. Li, X. N. Gu, S. Q. Lou, Y. F. Zheng, Biomaterials 2008, 29, 1329.
- [33] T. Kokubo, H. Takadama, Biomaterials 2006, 27, 2907.





- [34] Y. Zhao, M. I. Jamesh, W. K. Li, G. S. Wu, C. X. Wang, Y. F. Zheng, K. W. K. Yeung, P. K. Chu, Acta Biomater. 2014, 10, 544.
- [35] C. G. Overberger, M. Morimoto, J. Am. Chem. Soc. 1971, 93, 3222.
- [36] F. Shima, T. F. Uto, T. Akagi, M. Akashi, *Bioconjugate Chem.* 2013. 24. 926.
- [37] I. Zhitomirsky, Adv. Colloid Interface Sci. 2002, 97, 279.
- [38] P. Sarkar, P. S. Nicholson, J. Am. Chem. Soc. 1996, 79, 1987.
- [39] J. Lyklema, Adv. Colloid Interface Sci. 1968, 2, 65.
- [40] N. K. Nga, L. T. Giang, T. Q. Huy, P. H. Viet, C. Migliaresi, Colloids Surf. B 2014, 116, 666.
- [41] J. Luo, Q. Zhou, J. Sun, J. Q. Jiang, X. Zhou, H. W. Zhang, X. Y. Liu, J. Polym. Sci., Part A: Polym. Chem. 2012, 50, 4037.
- [42] J. Q. Jiang, Q. Z. Shu, X. Chen, Y. Q. Yang, C. L. Yi, X. Q. Song, X. Y. Liu, M. O. Chen, *Langmuir* 2010, 26, 14247.
- [43] Y. Gong, A. M. Zhu, Q. G. Zhang, Q. L. Liu, RSC Adv. 2014, 4, 9445.
- [44] R. Baskar, D. Kesavan, M. Gopiraman, K. Subramanian, RSC Adv. 2013. 3, 17039.

- [45] V. Ramkumara, S. Anandhib, P. Kannana, R. Gopalakrishnan, RSC Adv. 2015, 5, 586.
- [46] R. Baskara, D. Kesavanb, M. Gopiramanc, K. Subramanian, Prog. Org. Coat. 2014, 77, 836.
- [47] N. J. Ostrowski, B. Lee, A. Roy, M. Ramanathan, P. N. Kumta, J. Mater. Sci.: Mater. Med. 2013, 24, 85.
- [48] R. Y. Zhang, S. Cai, G. H. Xu, H. Zhao, Y. Li, X. X. Wang, K. Huang, M. G. Ren, X. D. Wu, Appl. Surf. Sci. 2014, 313, 896.
- [49] R. C. Zeng, A. G. Liu, F. Zhang, S. Q. Li, H. Z. Cui, E. H. Han, J. Mater. Chem. A 2014, 2, 13049.
- [50] Y. J. Lu, P. Wan, B. C. Zhang, L. L. Tan, K. Yang, J. X. Lin, Mater. Sci. Eng. C 2014, 43, 264.
- [51] J. C. Zhou, X. Z. Zhang, Q. Li, Y. Liu, F. N. Chen, L. Q. Li, J. Mater. Chem. B 2013, 1, 6213.
- [52] F. Feyerabend, J. Fischer, J. Holtz, F. Witte, R. Willumeit, H. Drücker, C. Vogt, N. Hort, Acta Biomater. 2010, 6, 1834.
- [53] E. Groos, L. Walker, J. R. W. Masters, Cancer 1986, 58, 1199.
- [54] W. H. Ma, Y. Z. Zhang, Chin. J. Tissue Eng. Res. 2014, 18, 432.
- [55] Y. Zhao, M. I. Jamesh, W. K. Li, G. S. Wu, C. X. Wang, Y. F. Zheng, K. W. K. Yeung, P. K. Chu, Acta Biomater. 2014, 10, 544.

